Heliyon 8 (2022) e09171

Contents lists available at ScienceDirect

Heliyon

journal homepage: www.cell.com/heliyon

Research article

Technological insights on the Early-Middle Bronze Age pottery of Monte Meana cave (Sardinia, Italy)

Giacomo Paglietti [a,b], Giuseppa Tanda [c,d], Rita Teresa Melis [e], Anna Musinu [e,f], Gabriele Cruciani [e], Marcello Franceschelli [e], Carla Cannas [e,f], Valentina Mameli [e,f,*], Mariano Casu [g]

[a] Museo Civico Archeologico di Santadi, Italy
[b] Museo Civico Archeologico "Genna Maria", Villanovaforru, Italy
[c] Dipartimento di Storia, Beni Culturali e Territorio, Università di Cagliari, Italy
[d] CeSim/APS, Sassari, Italy
[e] Dipartimento di Scienze Chimiche e Geologiche, Università degli Studi di Cagliari, Italy
[f] Consorzio Interuniversitario Nazionale per la Scienza e Tecnologia dei Materiali (INSTM), Cagliari Unit, Italy
[g] Dipartimento di Fisica, Università degli Studi di Cagliari, Italy

ARTICLE INFO

Keywords:
Sardinia
Bronze age
Pottery
Petrography
Infrared spectroscopy
X-ray diffraction
Firing temperature

ABSTRACT

An important Bronze Age settlement was discovered during an archaeological excavation in the Monte Meana karst cave in south-western Sardinia (Italy) between 2007 and 2012. In this region, the caves were used since the Neolithic for different purposes, such as burials or other rituals. The dig highlighted a rare example of domestic use of a cave and showed a case study of household space of the Early -Middle Bronze Age, at the beginning of the Nuragic civilization. This provided the opportunity to investigate through a multidisciplinary approach, the empirical knowledge of ancient potters and technological characters of local pottery production especially in relation to domestic use, in a context at that time devoid of external cultural interferences. For this purpose, a selection of 24 pottery sherds related to vessel forms for cooking, storage, and eating were studied through macroscopic surveys and archaeometric analysis by petrography, scanning electron microscopy, X-ray powder diffraction, and Fourier transform infrared spectroscopy. The results revealed some discriminant variables (shape, wall thickness, features of the paste, surface smoothing, presence of diagnostic mineralogical phases, and tempers), within the ceramic products of this Sardinian Bronze Age site, showing skillful management of firing temperatures.

1. Introduction

Sardinia is the second-largest island in the Mediterranean Sea. Between the 6th and 4th millennia, the island played an important role in the western Mediterranean for the exploitation and processing of its raw materials, such as obsidian [1, 2, 3] and copper, silver, and lead during the Chalcolithic Age [4, 5]. At the end of the 3rd millennium, Sardinia was affected by the Bell Beaker culture (named due to the typical inverted-bell beaker vessel), a prehistoric phenomenon identified in many parts of Western Europe [6]. In Sardinia the Beaker culture was documented during the Early Bronze Age (2200-1800 cal BC), in the same period of the Bonnanaro culture [7], and it was also culturally connected to Corsica and the Polada culture of northern Italy.

Starting from the Middle Bronze Age (1800-1350 cal BC), an important civilization, characterized by cyclopean stone towers called *nuraghi,* emerged and developed [8] without the apparent influence of external cultures. The Nuragic civilization, for its complexity and extraordinary ability to build stone monuments, represents one of the most important Bronze Age civilization of the Western Mediterranean area [9]. During the Late Bronze Age (1350-1200 cal BC) the island, as well as the southern coasts of the Italian peninsula, was a destination of Mycenaean and Levantine traders [10]. In these areas the discovery of *emporia* with Mycenaean, Cretan and Cypriot artifacts are evidence of an advanced network between the Near East and the Tyrrhenian area. Archaeometric research on Bronze Age pottery (for a review see [11, 12, 13]) has been fundamental to understanding the relationship between Nuragic and

* Corresponding author.
E-mail address: valentina.mameli@unica.it (V. Mameli).

https://doi.org/10.1016/j.heliyon.2022.e09171
Received 13 January 2022; Received in revised form 3 March 2022; Accepted 17 March 2022

Mycenaean and Levantine societies with an exchange of knowledge, proved by the imitation of Mycenaean pottery by the Nuragic people and, in other respects, by the Nuragic pottery discovered in Crete and Cyprus [14, 15, 16, 17, 18, 19]. Several authors studied the mineralogical composition and technological aspects of the Nuragic pottery, such as the Sardinian Late Bronze age gray ware [20] or general aspects of the Middle Bronze Age - Early Iron Age pottery, also in terms of evolution [14, 21, 22]. However, to date, no study has been carried out on the Sardinian pottery during the Early-Middle Bronze Age.

In this work we present an archaeometry study about household pottery found in the archaeological excavation of the Monte Meana cave. The archaeometric approach proposed is based on the combined use of different techniques: macroscopic observations, petrographic analysis, electron scanning microscopy (SEM), X-ray powder diffraction (XRPD) and Fourier transform infrared spectroscopy (FT-IR) [23]. To the best of our knowledge, the archaeological site of Monte Meana cave, dated by ^{14}C analysis between Early and Middle Bronze Age, represents the only case of a domestic use identified inside a cave during the period of transition towards the Nuragic Age. Moreover, it represents a moment of exclusive local production due to the absence of external influences. Therefore, the household pottery context of Monte Meana provides a good opportunity to study some technological characters of local handwork providing significant data at the protohistoric pottery studies in Sardinia.

2. Geological and geomorphological setting

The subject area of this research is the historical region of Sulcis, in south-western Sardinia, Italy (Figure 1a). The Sulcis region belongs to the External Zone of the Variscan chain in Sardinia [24]. Here, an angular unconformity (Sardic Phase) separates an underlying Lower Cambrian–Ordovician sequence from overlying transgressive Ordovician conglomerates ("Puddinga" Auct.). The Palaeozoic rocks are subdivided into a pre-Sardic sequence made up of the Nebida, Gonnesa and Iglesias Groups ranging in age from Lower Cambrian to Lower Arenig and post-Sardic sequence (Monte Argentu Formation and Pala Manna Complex) from Middle Arenig to Carboniferous [25]. The Palaeozoic rocks outcropping nearby the Monte Meana cave are Cambrian metasandstone/metasiltite and metalimestone/metadolostone belonging to the Nebida and Gonnesa Formations, respectively (Figure 1b). They are characterized by very low-to low-grade Variscan metamorphism [26]. The Palaeozoic rocks are intruded by granites of Carboniferous age. Around the cave, the Palaeozoic rocks are covered by the Miocene conglomerate and by rhyolitic rocks belonging to the oligo-miocene volcanic cycle of Sardinia. Rock fragments and pebbles from all the above mentioned lithologies are also found in the fluvial, eluvial/colluvial deposits and in the debris (see Figure 1b). The geomorphological context of the Paleozoic substratum is characterized by steep reliefs affected by water erosion and slope processes, while gentle hills are located on the Cenozoic volcanic and conglomerate substratum. Extensive dissected alluvial fans surround the alluvial plain of the river Riu Mannu that is characterized by alluvial terraces and paleosols. Intense karst processes affect the limestone rocks.

3. The archaeological setting: the Monte Meana cave

The karstic cave of Monte Meana (39°2′28″N, 8°42′31″E, 236 m a.s.l.) is located in the Cambrian carbonatic–dolomitic outcrop, 4 km from the center of the village of Santadi in south-western Sardinia, Italy. The cave has been inhabited from the Middle Neolithic to the Bronze Age. In the middle of the last century (1960s), alabaster quarrying activity modified the morphology of the cave and destroyed most of the archaeological *strata* within it. However, the five seasons of archaeological excavations (2008–2012), conducted by the Department of History, Cultural Heritage and Territory of the University of Cagliari (Italy), evidenced the presence of a residual archaeological deposit in an area of 50 m^2, not damaged by modern quarrying activities [27, 28, 29, 30] (Figure 2a,b). In the south side of the cave under 1 m of debris a small domestic activity area has been found. This is characterized by four archaeological layers (Figure 2a). The upper one is formed by approximately one hundred

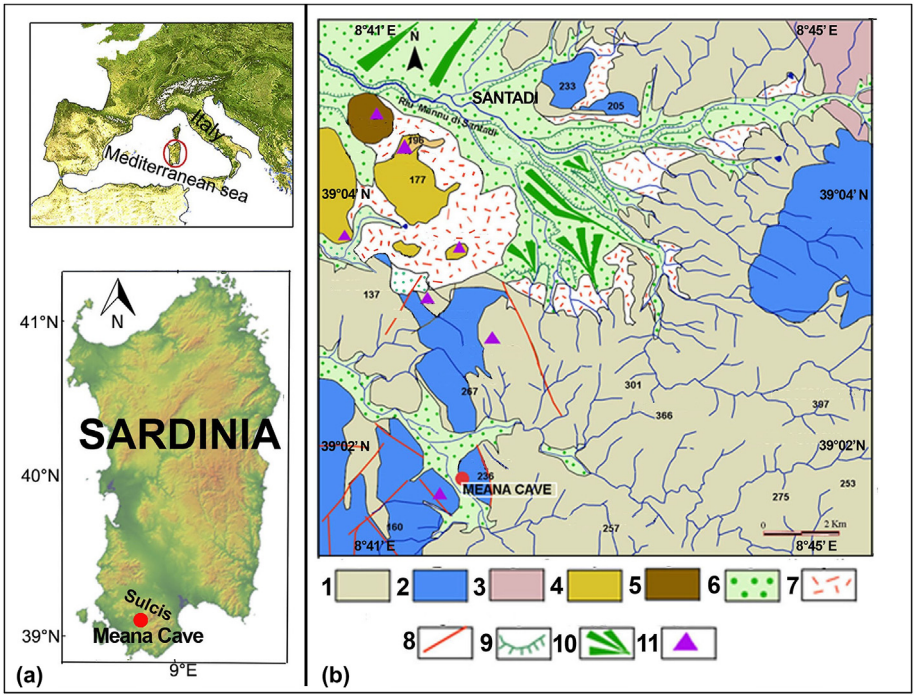

Figure 1. a) Location of the study area in the southern-west Sardinia; b) Schematic geological map of the study area; 1: metasandstone and metasiltite (Cambrian), 2: Metalimestone and metadolostones (Cambrian), 3: Granite (Carboniferous), 4: Conglomerates (Miocene), 5: Volcanic rock (Miocene), 6: Fluvial deposits (Quaternary), 7: Debris slope and eluvial/colluvial deposits, 8: Fault, 9: Fluvial terraces, 10: Alluvial fan, 11: Bronze age site (Nuraghi).

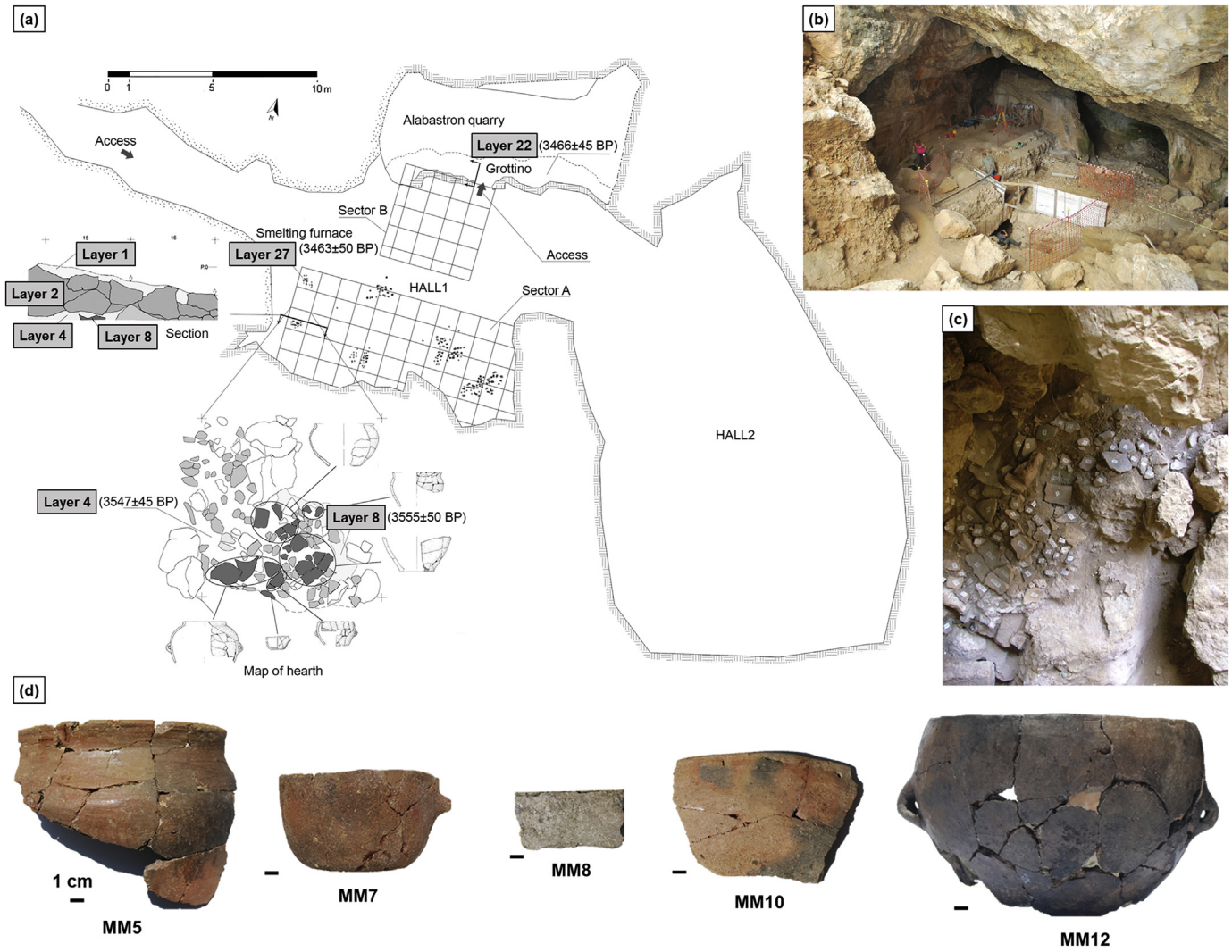

Figure 2. Planimetry (a), photo (b) of the Monte Meana cave, location of the archaeological findings (c) and images of some of the restored ceramic vessels (d).

sherds of ceramic paste, animal bones, lithic and bone tools, and carbonized seeds (layer 4). Among the one hundred ceramic sherds, those selected for this study have been restored to obtain some complete vessels (Figure 2a,c,d). The layer at the bottom refers to an area of 50 cm in diameter of different levels of overlapped ashes (layer 8) that suggests the presence of a hearth. A few meters from this hearth area, two other relevant archaeological layers have been found during 2012: a little copper smelting furnace (layer 27) [29], and, inside a small cave, a layer of charred soil with numerous carbonized seeds (layer 22) [27].

The ^{14}C measurements of these four layers, analysed by the software OxCal [31], dated back to a range 2026-1641 cal BC (Table 1), between the Sardinian Early Bronze Age and the Middle Bronze age.

4. Materials and methods

Monte Meana potteries are characterized by coarse ware, rich of impurities and granular constitution and classified as ceramic paste. To obtain an overview of the Monte Meana pottery, twenty-four sherds out of one hundred were selected on the basis of macroscopic parameters (such as surfaces treatment, color, wall thickness).

The archaeometric study was then performed on these twenty-four ceramic sherds, labelled with the code MM (Monte Meana). Seven of these sherds derive from complete vessel forms: one mug (MM7), two bowls (MM2, MM5), one skillet (MM10), one cooking pot (MM12) and two jars (MM3, MM8) (some images of these complete vessels are

Table 1. The ^{14}C data of the Monte Meana cave (Sardinia). For the analysis of the chronological information the program OxCal was adopted (OxCal version 4.2.4, reference [31]; r:5; atmospheric data from [32]).

Layer	Location	Laboratory code	Sample	^{14}C dates (BP)	$\delta^{13}C$ (‰)	Calibrated age (BC)	
						68.20%	95.40%
22	Small cave	LTL6006A	seed	3466 ± 45	−24.4 ± 0.1	1879–1696	1914–1641
27	Smelting furnace	LTL6007A	charcoal	3463 ± 50	−24.6 ± 0.2	1880–1730	1920–1660
4	Hearth	LTL4198A	charcoal	3547 ± 45	-25.5 ± 0.5	1951–1777	2017–1751
8	Hearth	LTL4199A	charcoal	3555 ± 50	-18.8 ± 0.5	1973–1778	2026–1743

provided in Figure 2d). Five ceramic fragments (MM1, MM4, MM6, MM9, MM11), which cannot be ascribed to any vessel form, were studied due to visual similarities with the first seven samples. Another twelve small sherds were selected randomly (MM13-MM24). Macroscopic observation and petrographic analyses were performed on the seven fragments from the complete vessels, and on the five ceramic fragments. FT-IR were performed on all the twenty-four samples. XRPD measurements were performed on one sample representative of each fabric. The sample MM7, an intact artifact, for conservative reasons was subjected only to FT-IR analysis. The adopted characterization approach and the list of the samples are provided in Fig. S1 and Table S1.

4.1. Macroscopic observation

The macroscopic analysis of the specimens was conducted with the aid of magnifying lenses for the description of the clay matrix (color, compactness and inclusions) and the surface treatments, to identify the specific use of the artefacts. The colors of the mixtures were described according to the Munsell Soil Chart [33].

4.2. Optical microscopy by thin-section analyses

Sample slices prepared in thin sections were investigated by the polarizing microscope in plane polarized light and crossed polars for the determination of the main forming minerals that are recognizable at the microscopic scale. The analysis of the sherds as thin sections was carried out by an optical polarizing microscope (LEICA DM 750 P with digital Color Camera LEICA EC3) working with single and crossed polars (magnification objectives: 2.5x, 1.25x, 10x, and 40x). It is based on the recognition of the nature, the microstructure, the relations of shape and size among the different components of the matrix, with the aim of defining homogeneous petrographic groups for microstructure of paste background, textural characteristics, and composition of the inclusions. Thin sections of the sherds were prepared using standard methods [34].

4.3. Scanning electron microscope analysis (SEM)

Scanning electron microscopy (SEM) investigation was performed with a ESEM Quanta 200 manufactured by FEI, equipped with a nitrogen-free Thermofisher EDS (energy dispersive spectroscopy) detector for X-ray microanalysis at Centro Servizi d'Ateneo per la Ricerca (CeSAR), University of Cagliari. Electron backscattered (EBS) imaging was used to characterize the microstructural features of the ceramic samples prepared in thin sections. The chemical composition of the minerals was determined by EDS–microanalysis.

4.4. Fourier transform infrared spectroscopy (FT-IR)

Fourier transform infrared spectroscopy (FT-IR) was adopted to identify the crystalline phases in the ceramic samples through the presence of the signals ascribable to their vibrational modes, in particular due to the higher sensitivity and speed of analysis in comparison with X-ray powder diffraction.

The infrared spectra were recorded in the mid IR region 400-4000 cm^{-1}, with a resolution of 4 cm^{-1}, using a Bruker Equinox 55. Representative FT-IR spectra were obtained by sampling about ten milligrams of sample and grinding the material using an agate mortar and pestle. The sampling was repeated twice in different areas of the sherd to ensure the obtainment of a representative sample. For the preparation of the KBr-based pellet, the samples were mixed with KBr in the proportion of 1:60 in weight and pressed to 10 tons for one minute. Because of the intrinsic complexity of the spectra, to remove the baseline shifts and emphasize small shoulders and peaks, second derivative IR spectra were also calculated.

4.5. X-ray powder diffraction analysis (XRPD)

As a supplementary investigation to support the results revealed by FT-IR analysis, the XRPD was used for the determination of the mineralogical phases, based on their crystalline structure. The analysis was carried out using a conventional θ-θ Bragg–Brentano focalizing geometry Seifert x3000, Cu Kα wavelength (λ = 1.54056 Å), graphite monochromator on the diffracted beam, and scintillation counter, in the angular range 8–60° 2θ with a step of 0.01° θ. A low amount (few mg) of the most representative sherds were powdered in an agate mortar and deposited on a Silicon zero-background sample holder. Rayflex Analyze software was used for qualitative analysis of the XRPD patterns.

5. Results

5.1. Macroscopic observation

On the basis of the macroscopic characters observed in the sherds as color, homogeneity and compactness of the paste, type of tempers and modality of treatment surfaces, five pottery groups, corresponding to the different vessel forms, were recognized and named as: Group A, Group B, Group C, Group D, and Group E (Figure 3a-e). The other five ceramic fragments (MM1, MM4, MM6, MM9, MM11), which were not directly ascribable to any vessel form, were added to the different groups based on similar macroscopic features. These observations are summarized in the Supplementary Material (Table S2).

Group A (MM1, MM2, MM3, MM4, MM7, MM11). This group of samples is characterized by a compact and homogeneous yellowish red (5YR 4/6) paste, with some small light white rock inclusions (with diameter smaller than 1 mm) and many large rock fragments with different colors (sizes of up to 4 mm). Voids are rare. The external and internal surfaces of MM3 appear both treated with polishing tools. Samples MM2 and MM7 show porous inner surfaces smoothed by hand. They are characterized by dark reddish brown (5YR 4/2) and reddish brown (5YR 5/4) colors, respectively. The wall thickness is about 7–7.5 mm.

Group B (MM5, MM6, MM9). This group is characterized by a compact and homogeneous light reddish brown (2.5YR 5/6) paste, with a few light inclusions (about 2 mm in diameter) and grey rock fragments (sizes of up to 2 mm). Voids are present in vesicular forms. The external surface appears grey (7.5YR 6/1), while the internal side is lightly bluish gray (Gley 2 7/5 PB) and both appear polished by tools (MM 5). The wall thickness is about 13 mm.

Group C (MM12). This sample shows a compact but inhomogeneous paste with greyish brown (10YR 5/2), reddish yellow (5YR 3/6) and grey (2.5YR 5/1) zones. It is characterized by numerous white, yellow and pink inclusions (smaller than 3 mm). Voids are almost absent. The external surface is greyish brown (10YR 5/2) and burnished while the internal one is reddish brown (2.5YR 5/4) and smoothed by hand. The bottom of the pot has a strong abrasion probably due to a prolonged exposure to fire. The wall thickness is about 8 mm.

Group D (MM10). This sample is characterized by a highly homogeneous internal red color zone (2.5YR 6/6) and by a reddish grey (2.5YR 5/1) external zone. Numerous white and grey inclusions smaller than 4 mm are clearly visible in the paste and yellow ones in the external zone. Voids are present in vesicular forms. The external surface (reddish grey, 2.5YR 5/1) appears polished by tool while the internal one (light red, 2.5YR 6/6) is smoothed by hand. The wall thickness is about 10 mm.

Group E (MM8). This sample is characterized by a very homogeneous grey paste (Gley1 5/N) with a low number of small (about 1 mm) white inclusions and many other ones with different color, like yellow inclusions of different size (up to 5 mm) that appear at the internal surface. Numerous ellipsoidal voids, probably attributable to the presence of organic material, are also observable. External and internal surfaces appear grey (Gley1 5/N) and smoothed by hand. The wall thickness is about 15 mm.

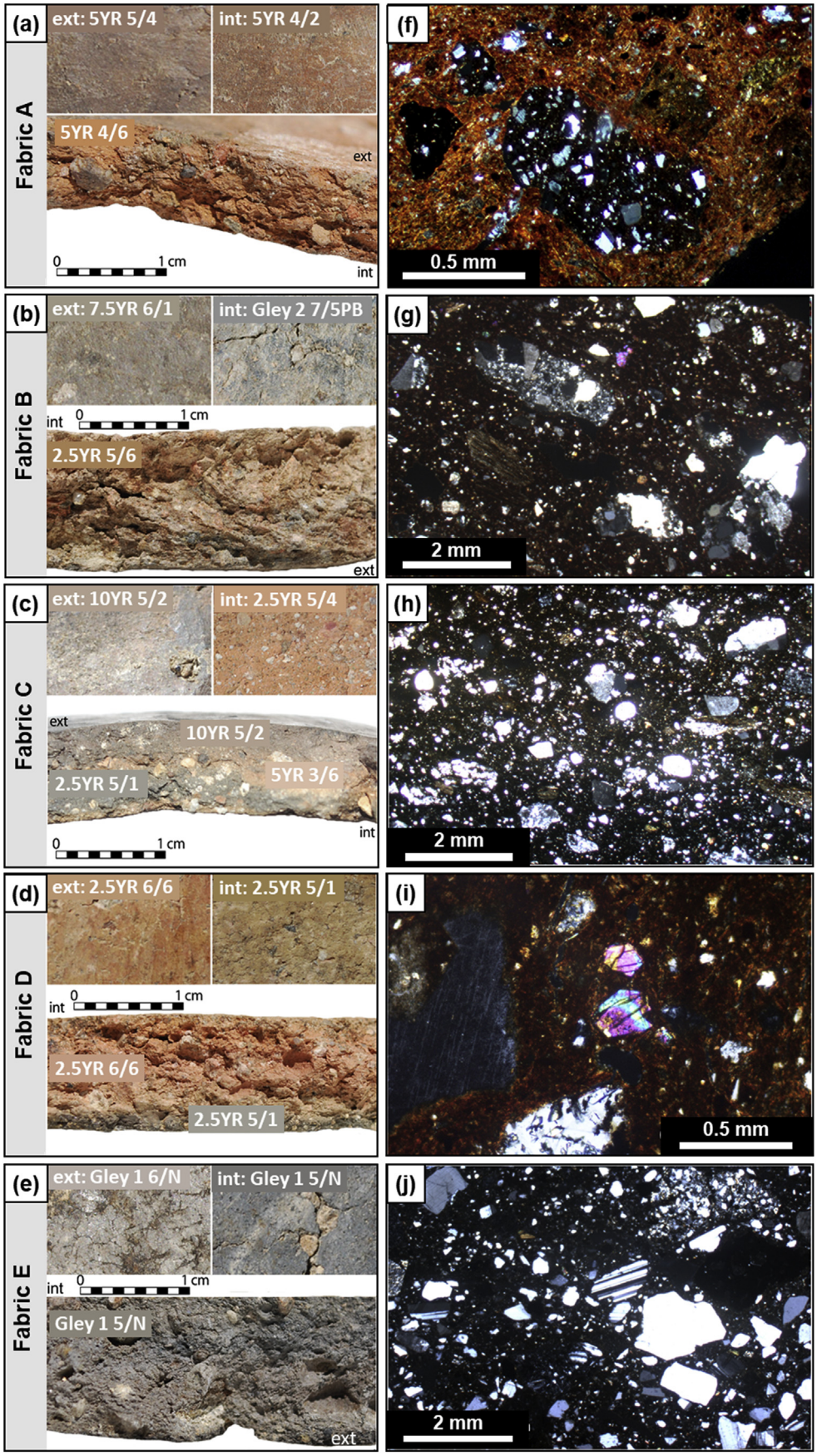

Figure 3. Section and surfaces of investigated pottery groups by macroscopic observation (a–e). For each group, images of the external (ext), internal (int) surfaces and the section are provided, together with the color codes assigned on the basis of the Munsell Soil Chart (2000). Photomicrographs of thin sections of Monte Meana pottery (f–j). f) Fabric A: grog of the sample MM1 (XPL, 10x); g) Fabric B: metamorphic rock inclusions in the sample MM5 (XPL, 1.25x); h) Fabric C: rounded quartz grains of the sample MM12 (XPL, 1.25x); i) Fabric D: olivine and metamorphic rock inclusions in the sample MM10 (XPL, 10x); j) Fabric E: quartz, plagioclase and K-feldspar in the sample MM8 (XPL, 2.5x).

5.2. Petrographic and electron microscope analysis

Petrographic analysis at the polarizing microscope has allowed to identify five fabrics (A, B, C, D, E) (Figure 3f-j, Table S3, Fig. S2) that correspond to the five groups evidenced by macroscopic observation (Figure 3a-e). The results are summarized in the Supplementary Material (Table S3).

Fabric A (MM1, MM2, MM3, MM4, MM11). All the samples show a mineral fraction with angular and sub-angular grains of quartz, K-feldspars, muscovite and spheroidal rust brown nodules probably composed by femic minerals. Moreover, metamorphic rock fragments (metasiltite and metasandstone) and weathered fine-grained rock fragments of sericite are observed. Magmatic rock fragments (granite) and rare limestone fragments are observable in the samples. Grogs are attested in the clay matrix of all samples (Figure 3f). Vesicular and lenticular voids are present too.

Fabric B (MM5, MM6, MM9). The mineral fraction presents subangular grains of quartz, K-feldspars and muscovite (Figure 3g). Metamorphic (metasandstone and metasiltite) and magmatic rock (granite) inclusions and rare limestone fragments are evidenced. Few grogs are attested in the paste. The clay matrix has vesicular voids.

Fabric C (MM12). MM12 shows a mineral fraction characterized by several rounded quartz grains, K-feldspars, metamorphic and limestone fragments (Figure 3h). Some vesicular voids are visible.

Fabric D (MM10). MM10 shows rare quartz crystals, few plagioclase and K-feldspars, pyroxene and olivine, and metasandstone and metasiltite fragments (Figure 3i). No voids are observed.

Fabric E (MM8). MM8 is characterized by numerous angular quartz, K-feldspars (microcline, sanidine and anorthoclase), zoned plagioclase, and a few amphibole and muscovite crystals. Metamorphic and volcanic rock fragments are present (Figure 3j). Few voids are observed.

The clast/matrix ratio for all the fabrics has been qualitatively estimated by visual observation at the scanning electron microscope (Figure 4). On a textural basis it is possible to distinguish polymineralic aggregates (>200 μm in size), medium-to coarse-grained single crystals, and rock fragments embedded in a fine-grained (<50 μm) matrix.

Fabric A (MM4, MM11). The clast/matrix ratio is ~15–20%. Whitish and black aggregates up to 4–5 mm in size are embedded into a fine-grained, predominant reddish matrix, so that the overall color of the samples is red. The aggregates are (i) Ti-oxide + chlorite and (ii) quartz + white mica + chlorite + Fe/Mn-oxide (Figure 4a). White mica tabular grains, intimately intergrown in a microstructure similar to interleaving with chlorite and albite, are 300–350 μm in length (Figure 4b). Plurimillimetric quartz grains with inclusions of euhedral Fe-oxide were also observed. K-feldspar crystals sometimes show perthitic exsolutions. In a few samples, biotite was also found as medium-grained single crystals and/or in small flakes in the matrix. The surrounding matrix is mainly made up of quartz, feldspar (albite, K-feldspar, and alkali-feldspar) and phyllosilicate (sericite and subordinate chlorite, often in interleaving) and accessory Ti- and Fe/Mn-oxide. Igneous rock (granite) and rare limestone fragments have been found in the samples. The samples are porous, with elongated, lenticular voids visible by naked eye.

Fabric B (MM5, MM9). Clast/matrix ratio ranges between 15-30%, depending on the specific sample. Most of the aggregates (or coarse-grained crystals) are whitish to light-colored, with black ones being strongly subordinate. The coarse-grained minerals are prismatic K-feldspar (up to 1 mm in size) and rounded quartz of comparable size. The mineral aggregates consist of: (i) deformed and kinked, white mica grains up to 0.5 mm in length growing with smaller and subordinate chlorite and albite (Figure 4c) very similar to those described in Fabric A samples; (ii) plurimillimetric and fractured, homogeneous in composition, K-feldspar partially recrystallized into a fine grained aggregate of albite and polygonal quartz (Figure 4d); (iii) anhedral, altered and partially recrystallized Ca-rich mineral (grossular/epidote) in plurimillimetric coarse-grained crystals, or in smaller ones in the matrix; (iv) anhedral and shapeless, 300 to 400 μm-sized aggregates of fine-grained iron oxides. The fine-grained matrix that hosts the above-mentioned coarse-grained crystals and aggregates mainly consists of albite, quartz, K-feldspar, chlorite, muscovite, chloritized biotite, epidote, kaolinite, and Ti/Fe-oxide. Biotite/chlorite and muscovite/biotite interleaving have been observed in the matrix. Monazite occurs as accessory phase. Voids occurrence and abundance is significantly variable in the different samples from this fabric.

Fabric C (MM12). The clast/matrix ratio in the samples is ~20%. The samples sometimes show an alternation of blackish, brownish and reddish layers. The mineral fraction consists of several rounded quartz grains, and of millimetric, prismatic K-feldspar and albite crystals (the latter by far longer than 1.0–1.5 mm in length). Rock fragments as well as rounded aggregates of K-feldspar + quartz + epidote resembling refractory grogs up to 2–3 mm in size (Figure 4e) were also observed. Vesicular voids were also found.

Fabric D (MM10). The clast/matrix ratio is ~20%. Samples are characterized by a reddish color. They consist of rock fragments (up to 4–5 mm in size), rare aggregates and medium-to coarse-grained crystals in a reddish matrix. Rounded rock fragments (up to 2 mm in size, Figure 4f) derived from granite consist of quartz, perthitic K-feldspar and recrystallized plagioclase in various proportions. The aggregates are composite and consist as follows: i) rounded to subrounded aggregates of K-feldspar, albite, quartz, epidote, and chlorite; ii) epidote plus albite; iii) K-feldspar with subordinate blebs of albite and small biotite flakes; iv) quartz with subordinate K-feldspar and white mica; v) rounded aggregates of albite + quartz + white mica + chlorite. Isolated crystals within the matrix, up to 1 mm in size, are quartz, perthitic K-feldspar, and plagioclase. Quartz crystals, sometimes with resorbed edges, are similar to those occurring in volcanic rocks. Plagioclase millimetric single crystals are almost completely replaced by a Ca-rich phase (epidote) and/or significantly recrystallized into epidote plus quartz. Feldspars (mostly K-feldspar) include rounded quartz grains. Quartz, white mica, K-feldspar, alkali-feldspar, albite, biotite/chlorite interleaving, tremolite, and Fe/Ti-oxide were observed in the matrix. No voids were observed in the samples from this fabric.

Fabric E (MM8). The clast/matrix ratio is ~20–25%. Aggregates (and crystals) visible by naked eye are whitish, brownish or black, whereas the overall color of the samples is greyish to brownish. The texture consists of medium to coarse-grained (up to more than 3 mm in size) rounded and/or prismatic crystals of alkali-feldspars and plagioclase embedded in a slightly oriented fine-grained matrix (Figure 4g). Alkali-feldspar sometimes shows resorption edges at their interface with the matrix (Figure 4h). Quartz crystals show smaller size, usually not higher than 0.3 mm. Subhedral to euhedral crystals of Ti/Fe-oxide have dimensions comparable with those of quartz. The fine-grained matrix that surrounds the aforementioned crystals, consists of quartz, biotite, plagioclase, ilmenite, white mica, K-feldspar, alkali-feldspar, Fe/Ti-oxide, apatite and rare calcite. A few vesicular and lenticular voids are observed.

5.3. FT-IR

The FT-IR results of all the 24 samples (seven fragments of the complete vessels, five ceramic fragments and the twelve randomly selected sherds) are presented in Figure 5, Figures S3 and S4 on the basis of the previous classification of the fabrics (A, B, C, D, E). The assignments of the FT-IR absorption (Figures 5 and S4) and the second derivative bands (Fig. S3) have been made on the basis of the available literature of a great variety of minerals [35, 36, 37]. The main mineralogical phases that characterize the different potteries are quartz, K-feldspars (microcline and orthoclase) and phyllosilicates (kaolinite, talc, muscovite). Fayalite and gypsum, in small and different amounts, are also found in many samples of some fabrics. A report list of the relevant minerals is given in Table 2.

Fabric A (MM1, MM2, MM3, MM4, MM7, MM11). The FT-IR spectra together with the corresponding assignments are reported in Figure 5 and the second derivative of the IR absorption spectrum of the sample MM4 is

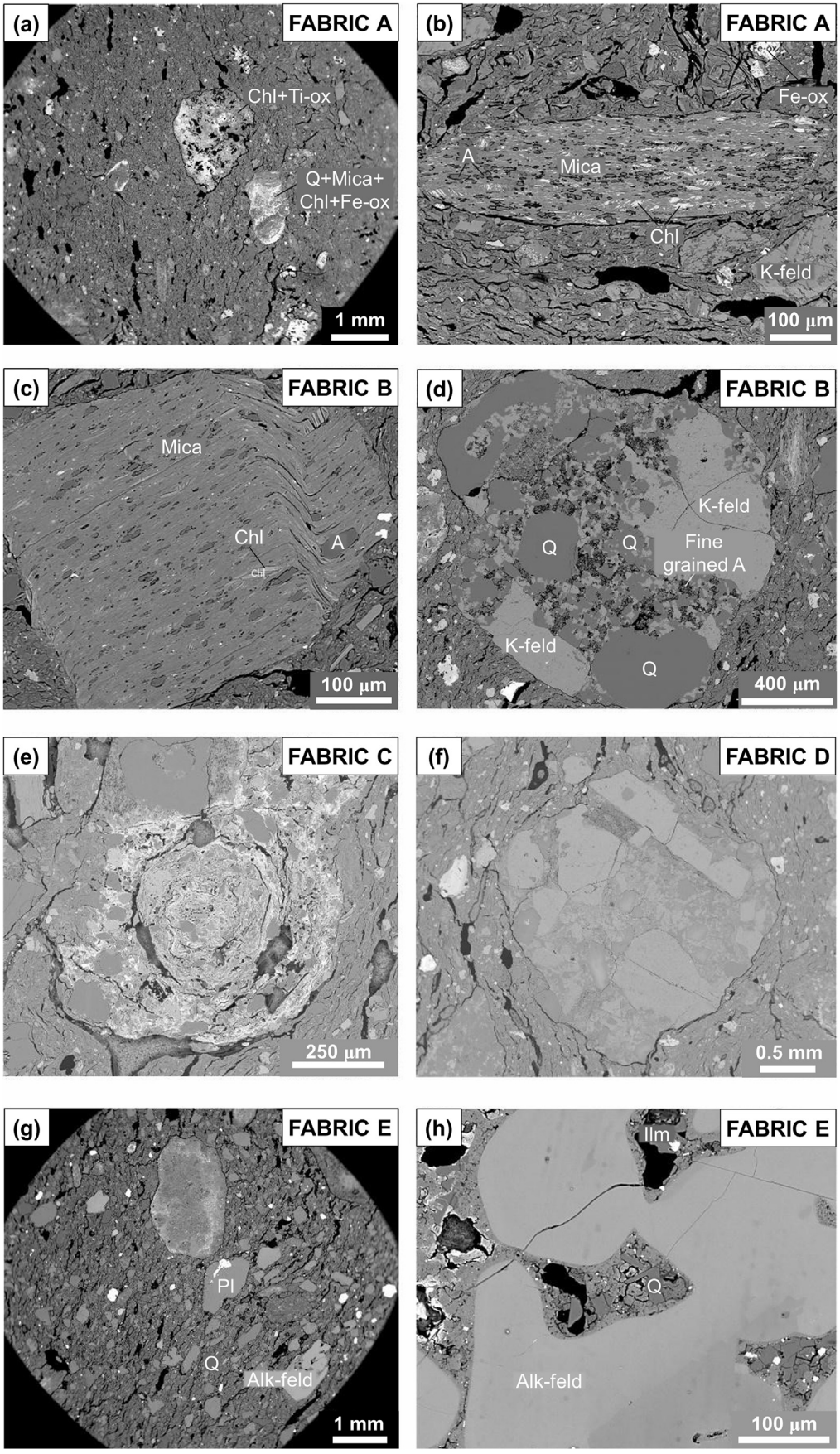

Figure 4. Electron backscattered (EBS) images of some petrographic fabrics of the ceramic products from Monte Meana cave. a) panoramic view of the matrix with Ti-oxide + chlorite and quartz + white mica + chlorite + Fe/Mn-oxide aggregates in Fabric A; b) White mica intimately intergrown with chlorite and albite in Fabric A; c) kinked white mica grain overgrown by smaller and subordinate chlorite and albite in Fabric B; d) partial recrystallization of K-feldspar into fine grained albite + quartz in Fabric B; e) Rounded refractory grog made up of quartz, feldspar and epidote in Fabric C; f) Rounded rock fragments derived from granite in Fabric D; g) panoramic view of alkali-feldspars and plagioclase in the matrix of Fabric E; h) resorption edges of alkali-feldspar in a ceramic product of Fabric E.

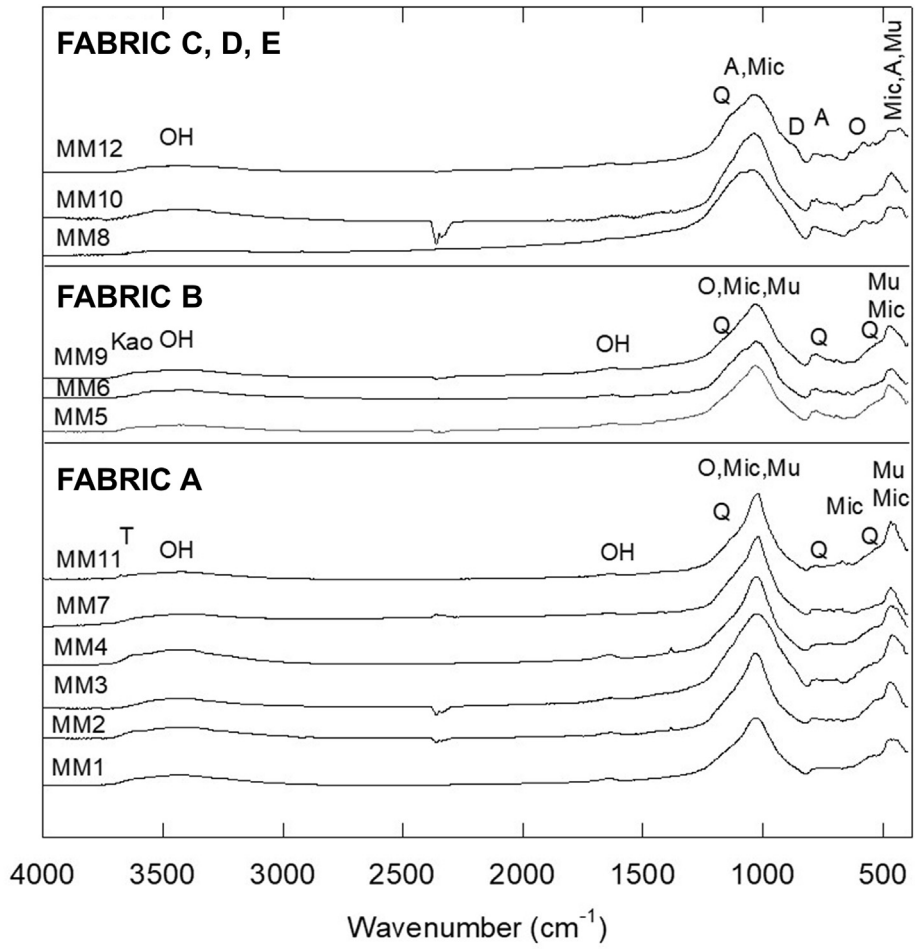

Figure 5. FT-IR absorbance spectra of the samples: MM1, MM2, MM3, MM4, MM7, MM11 (Fabric A); MM5, MM6, MM9 (Fabric B); MM12 (Fabric C), MM10 (Fabric D) and MM8 (Fabric E). Q = Quartz; Mic = Microcline; O=Orthoclase; Mu = Muscovite; A = Albite; D = Diopside; T = Talc.

Table 2. Mineralogical composition of the fabric of the sherds according to the FT-IR analysis. A = Albite; Cal = Calcite; D = Diopside; Fay = Fayalite; G = Gypsum; Kao = Kaolinite; K-feld = K-Feldspars (Orthoclase, Microcline); Mu = Muscovite; Q = Quartz; T = Talc; tr = trace. *low, ** medium and *** high amount.

Fabrics	Samples	Q	Kao	K-feld	Cal	A	Mu	Fay	D	G	T
A	MM1, MM2, MM3, MM4, MM7, MM11, MM13, MM16, MM19, MM20, MM22, MM23, MM24	**	-	*	-	-	*	-	-	*	*
B	MM5, MM6, MM9	***	**	*	-	-	*	-	-	*	-
C	MM12	***	-	**	tr	*	-	*	-	*	-
D	MM 10	**	-	**	-	*	-	*	*	*	-
E	MM8, MM14, MM15, MM17, MM18, MM21	**	-	**	-	*	*	-	-	*	-

shown in Fig. S3. All the samples of this fabric show the presence of adsorbed water (water OH- stretching at 3430 cm^{-1} and water H–O–H bending at 1638 cm^{-1}), quartz (bands at 1160 cm^{-1}, 1080 cm^{-1}, 797 cm^{-1}, 778 cm^{-1}, 695 cm^{-1}, 512 cm^{-1}, and 460 cm^{-1}), and K-feldspars (orthoclase at 1040 cm^{-1}, 1010 cm^{-1}, 770 cm^{-1}, 728 cm^{-1}, and microcline at 1140 cm^{-1}, 1010 cm^{-1}, 646 cm^{-1} and 585 cm^{-1}). Moreover, the absorption bands at 754 cm^{-1}, 553 cm^{-1} and 412 cm^{-1} in these samples are ascribable to muscovite [35]. Traces of gypsum are also found, as suggested by the peak at 667 cm^{-1} [38] in the profile of the second derivative (Fig. S3). The samples MM7 and MM4 (Figure 5) show two additional narrow absorption peaks at 3674 cm^{-1} and 588 cm^{-1} which indicate the presence of talc [37], as highlighted by the second derivative in Fig. S3.

Fabric B (MM5, MM6, MM9). The three samples of the Fabric B are characterized by quartz, muscovite, K- feldspars (microcline, orthoclase) and small amounts of gypsum are shown in Figure 5. In Fig. S3 the second derivative of the IR absorption spectrum of the sample MM6 is reported. A large band with a maximum centred at 3632 cm^{-1} is also present, which can be attributed to kaolinite [39, 40]. Its presence is also confirmed by the signals at 1117 cm^{-1}, 1033 cm^{-1}, 915 cm^{-1}, and 430 cm^{-1} in Fig. S3. The mineralogical composition of this fabric is very similar to the Fabric A, but richer in quartz, as evidenced by the intensity ratio (see band at 797 cm^{-1}), and without the talc phase.

Fabrics C (MM12), **D** (MM10) and **E** (MM8). These fabrics, each one represented by one sample, are all characterized by the presence of albite (1095 cm^{-1}, 1035 cm^{-1}, 588 cm^{-1}, and 425 cm^{-1}), absent in the other two fabrics, and by the absence of kaolinite commonly found in the samples of the Fabric B as shown in Figure 5 and Fig. S3. Quartz, K-feldspars (orthoclase, microcline) are also present in all the samples. Small bands at 832 cm^{-1} and at 959 cm^{-1} in the samples of fabrics C and D suggest the possible presence of small amounts of an olivine mineral like fayalite (Fe_2SiO_4), which is highlighted by the second derivatives in Fig. S3. Traces of gypsum are also found, as suggested by the peaks at 667 cm^{-1} and 595 cm^{-1} in the profiles of the second derivatives (Fig. S3).

Calcite is present as a trace in Fabric C. The Fabric D is characterized by a low percentage of quartz and by the presence of peaks at 967 cm^{-1}, 920 cm^{-1}, 865 cm^{-1}, and 670 cm^{-1} which can be ascribed to the presence of diopside [35, 41]. Muscovite has been found in Fabric E.

These results are in good agreement with petrographic observations for all the fabrics and allow us to confirm the presence of five different classes of materials used for the ware production.

In addition to these samples, twelve randomly selected sherds with small size were submitted to the FT-IR analysis (Fig. S4). Seven of these samples (MM13, MM16, MM19, MM20, MM22, MM23, MM24) are characterized by quartz, muscovite, K-feldspars (microcline, orthoclase). This composition allows to attribute these samples to Fabric A. Five of these samples (MM14, MM15, MM17, MM18, MM21), on the basis of the composition (quartz, muscovite, K-feldspars, albite), were attributed to Fabric E.

5.4. XRPD

In order to strengthen the mineralogical attributions identified by FT-IR and petrographic analysis, XRPD analysis was performed on a representative sample for each fabric (Figure 6). The investigation on the pottery samples confirms the presence of quartz and K-feldspars in different amount, in particular microcline and orthoclase, in all the samples. Muscovite has been identified in the Fabrics A, B and E, but it is absent in the C and D Fabrics, while high-albite and fayalite are present in the C, D and E Fabrics. The discrimination between high-albite, with a disordered Al–Si arrangement, and low-albite was possible thanks to the presence of an intense diffraction peak at about 27.8° (2θ), typical of high-albite, near the most intense one at 28° (2θ), in agreement with the powder diffraction files for these crystalline phases (PDF card # 00-010-0393 for high-albite; PDF card # 00-009-0466 for low-albite). Talc has been identified in the sample MM4, in agreement with FT-IR results. The presence of diopside in the sample MM10 (Fabric D) is confirmed. Neither gypsum nor kaolinite signals were identified in the investigated samples, probably due to amounts below the detection limit.

These observations, including the different crystallographic phases in relation to the techniques used (petrography, SEM, FTIR e XRPD), are summarized in the Supplementary Material (Table S4).

6. Discussion

The analyzed Monte Meana pottery (2026-1743 BC) followed the Bell Beaker culture of the Calcolithic/Early Bronze Age (2400-2000 BC) and was contemporary to the beginning of the Nuragic Age (Middle Bronze Age, 18th century BC). The Beaker culture was characterized by a good quality and standardized pottery production [42, 43] and its typical features were kept in the local production of Sardinian pottery until the Early Bronze Age (2200-1800 BC). This fact is probably due to the exchange of knowledge and techniques between the island and the Beaker European culture [6]. However, once the Beaker influence came to an end, the craft production of the Monte Meana, as observed for other Sardinian Bronze-Age contexts [44], showed the absence of

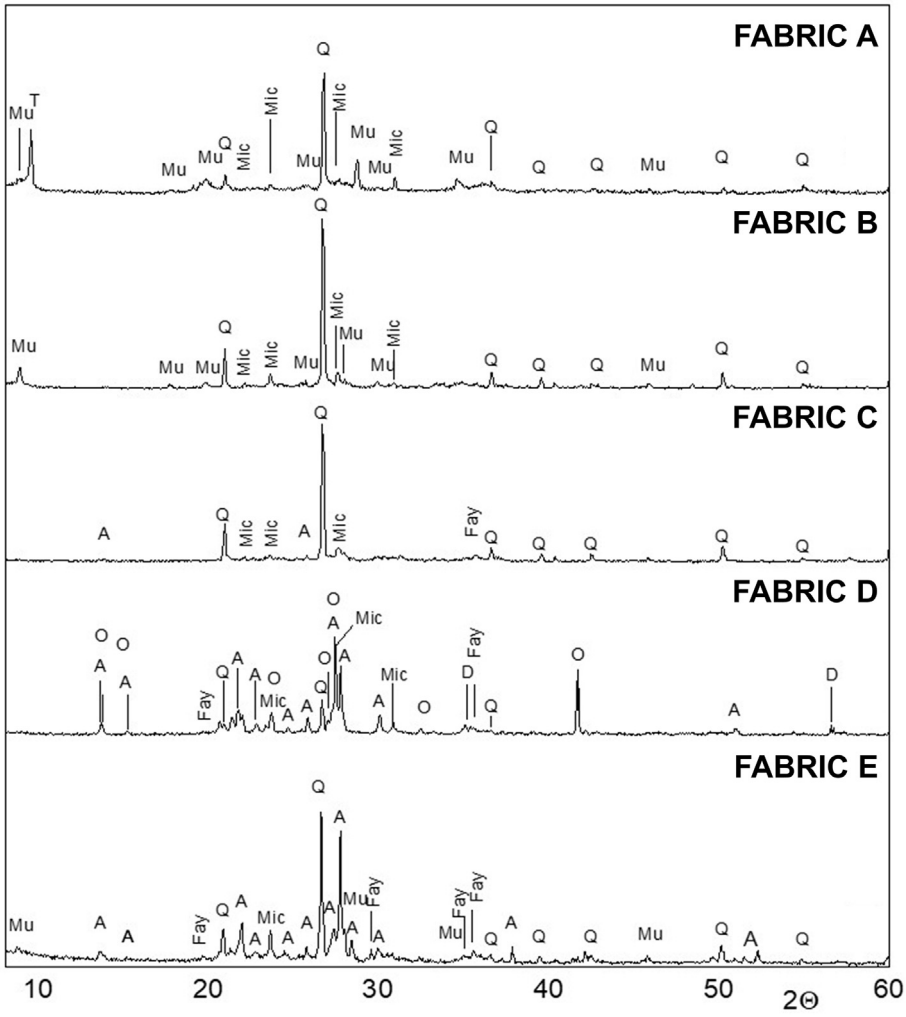

Figure 6. XRPD patterns of representative samples: MM4 (Fabric A), MM5 (Fabric B), MM12 (Fabric C), MM10 (Fabric D), MM8 (Fabric E). A = Albite; D = Diopside; Fay = Fayalite; Mu = Muscovite; Mic = Microcline; O=Orthoclase; Q = Quartz; T = Talc.

Table 3. Evaluation of the firing temperatures and possible functions of the Monte Meana potteries on the basis of the formation/transformation temperatures associated with the mineralogical compositions obtained by FT-IR/XRPD analyses. The symbol X has been used to indicate the technique that revealed to be useful for the evaluation of the firing temperatures.

Fabric	Marker of thermal Change	Temp. [1]	FT-IR	XRPD	Estimated Firing Temperature (T_F)	References	Function compatible with the mineralogical composition	Function compatible with the macroscopic observation
A	Phase: Talc Phenomenon: Dehydroxylation and decomposition	800–850 °C	X	X	<850 °C	Zhang *et al.* 2006 [52]	*n.d.*	solids or liquids storage
B	Phase: kaolinite Phenomenon: Dehydroxylation	425–675 °C	X	-	<675 °C	Elsass and Oliver 1978 [53]	cooking	cooking, solids or liquids storage
C	Phase: Albite (presence) Ca-silicates (absence) Phenomenon: Formation	<850 °C	X	-	≤850 °C	Maritan *et al.*2006 [54]	cooking	cooking
D	Phase: Diopside (Ca-silicates) Phenomenon: Formation	>850 °C	X	X	>850 °C	Maritan *et al.*2006 [54]	serving and eating, solids or liquids storage	serving and eating
E	Phase: High Albite (Ca-silicates) Phenomenon: Formation	>750 °C	X	X	≥850 °C	Maggetti 1981 [55], De Benedetto *et al.*, 2002 [35]	serving and eating, solids or liquids storage	solids or liquids storage

[1] Range of temperatures or temperatures at which the mineralogical phase undergoes a transformation. n.d. means not determinable.

standardization and production of "prestige vessel". Instead, a return to a standardization and high quality of some vessel forms occurred during the Late Bronze Age (1450-1200 BC) when the Nuragic civilization met the Levantine people [14].

Many studies in the literature are devoted to the adoption of a classification of archaeological pottery based on the relationship between the macroscopic parameters (shape, surface treatment, wall thickness and use-wear) and the function in contemporary African tribes [45, 46, 47]. For instance, in a recent study, this approach allowed the authors to identify the household function of the ceramic vessels from the 7th millennium cal. BC Yarmukian sites [48], located in the historical region of Galilee and Jordan valley, in the Israel, Cisjordan and Jordan territories, for instance by associating wall thickness higher than 12 mm to long-term storage, whereas medium and fine wall thicknesses were found for short-term storage and serving/eating functions. However, the identification of the functions was achieved by the combination of the different macroscopic parameters. Moreover, some of the macroscopic features (*e.g.* wall thickness) can be associated with the mechanical or thermal properties of the vessels, suggesting their specific applications, *i.e.* cooking *versus* storage functions [45]. Similarly, specific mineral phases or types of rocks are often added to the ceramic paste to control the physical properties of the ceramic products, among them angular quartz, plagioclase and various types of rock fragments (granite and limestone) [45, 49]. Furthermore, the use of talc is known to reduce the incidence of cracking on repeated household use [50]. In this context, this work provides a classification of the functions of Monte Meana pottery assemblage, in terms of food storage, transportation, preparation, cooking, serving and consumption.

The lithic inclusions found in all the five petrographic fabrics, consist of metasandstone/metasiltite, granite and limestone, with the occurrence of quartz, K-feldspars and muscovite that are very common minerals of felsic metamorphic rocks. These inclusions are compatible with the lithologies outcropping in the area nearby the cave of Monte Meana (Figure 1b), suggesting the availability of local raw materials suitable to produce ceramic manufacts.

The macroscopic observation of the vessels permits to evaluate the external characteristics of the paste, such as color, homogeneity, and consistency (Figure 3a-e, Table S2). Petrographic analysis shows, for all the samples, a common composition in terms of mineralogical phases and lithic inclusions (angular and rounded quartz, K-feldspars and rock fragments), and some differences that have allowed us their classification in the five fabrics. All the phases revealed by petrographic and SEM observations have been confirmed by FT-IR and XRPD analyses.

Fabrics A and B (bowls, a jar and a cup) show similar features: thin-medium wall thickness (from 7 to 13 mm) made up of a homogeneous paste with smoothed outer and inner surfaces. Taking into account that the thickness of the walls is strictly related to the size of the container and its intended use, we can assume that this feature together with the surface treatment strongly suggest their function as liquids storage. One sample (MM2, bowl of Fabric A) shows porous inner surfaces that suggest the use for heat processing. Fabric C is related to a pot with thin walls (8 mm) of an inhomogeneous paste with well–burnished external surfaces and an abraded bottom (probably due to a prolonged exposure to fire). These features can be associated to a cooking function. In fact, thin walls conduct heat better, allowing to cook food faster and saving fuel [45]. Fabric D is related to a skillet with medium thickness walls (10 mm) with a homogeneous paste and well-treated surfaces, which can be used for serving and eating. Fabric E is related to a big jar, showing thick walls (15 mm) of homogeneous color coarse paste with few voids. Thick walls are desirable to increase mechanical stability and to keep moisture in or out of the vessel, therefore this feature, accompanied with the vessel shape, is ideal for dried-food storage.

Based on the petrographic analysis: muscovite is found in the Fabrics A, B, and E; numerous plagioclase crystals have been observed in the Fabrics D and E while pyroxene and olivine are present only in the Fabric D and amphibole is present only in Fabric E; grogs are evidenced only in the Fabrics A and B. This latter aspect suggests an intentional addition of grogs in the ceramic paste to temper the pottery (*chamotte*) [9, 30, 45], as already observed in the literature by Early and Middle Bronze Age in vessels from north and central Sardinia [21, 22] and Sicily [51]. The presence of some mineralogical phases detected by petrographic analysis and other additional ones was also indicated by FT-IR and XRPD analyses (Table S4). In particular, talc was found, by these latter characterization techniques, to be present only in some samples in the Fabric A. The differences in the mineralogical composition among the fabrics suggest technological production strategies, which probably involve the use of different tempers. All the phases found in the different ceramic products can be considered useful markers of thermal changes. Among them, for each fabric, we have selected the mineralogical phase or phases that provide information about the firing temperature reached during the firing process (Table 3).

In the Fabrics A and B, the presence of quartz, K-feldspars and muscovite was identified, while kaolinite was found in the Fabric B and talc in Fabric A (Tables 2, S4). Talc phase is known to undergo dehydroxylation and decomposition at temperatures higher than 800 °C [52]. The dehydroxylation of kaolinite is claimed to occur between 425 °C and 675 °C by in-situ XRPD [56]. Several authors [39, 40, 53, 57, 58] observed that the treatment at 500 °C induces an important decrease on the intensity of the characteristic kaolinite bands in the 3700-3800 cm^{-1} region, due to the dehydroxylation of kaolinite, and the disappearance of the band at 915 cm^{-1}. At this temperature, only a weak broad band remains at about 3600 cm^{-1}. In our case, although the band at 3700-3800 cm^{-1} is very weak, the presence of the band at 915 cm^{-1} is an indication of kaolinite traces in Fabric B (Table 3) [59]. The other components (quartz, muscovite and K-feldspars) have a wider thermal stability window and are not useful for a diagnosis in these samples. In the Fabric C (Table 2), the presence of albite and probably calcite and the contextual absence of bands indicative of high temperature Ca-silicates suggest that the firing temperature in these cases is below 850 °C. In addition to temperature, atmosphere and exposure time to high temperature can significantly influence the decomposition behavior [45, 60]. Above 850 °C the calcite decomposition can induce the formation of the high-temperature crystalline phase (calcium and aluminium silicates) as gehlenite ($CaAl_2SiO_7$), diopside ($CaMgSi_2O_6$) and anorthite ($CaAl_2$–Si_2O_8). In the Fabric D, the presence of quartz and the occurrence of diopside, a firing mineral formed during firing process [35, 55], indicate a firing temperature higher than 850 °C [38, 61, 62]. In the Fabric E, quartz, muscovite, microcline and high albite are present while firing minerals, like diopside, are totally absent. Moreover, the presence of high albite, which is stable at $T > 750$ °C [63] suggests that the pottery was fired at a temperature close to 850 °C.

The firing temperatures suggested in this study provide additional elements to interpret the ceramics function. In fact, the firing process influences the technological properties of ceramics as a function of the thermal and mechanical behavior of the clay and tempers components. The low firing temperature (about 500 °C) contributes to increase the thermal stress resistance of the pottery, in agreement with a cooking use [45]. On the other hand, high temperature (850–900 °C) contributes to a weak thermal resistance but to a high mechanical stress resistance [45]. Therefore, for the Fabrics D and E, it is possible to exclude a cooking function according to the hypothesised firing temperatures, the thick walls and the vessel shape, while an application as dry storage, serving and eating could be ascribed to them. In the case of the Fabric B, the estimated low firing temperature make it compatible with a cooking use, despite the macroscopic features similar with respect to those of Fabric A (internal and external surfaces smoothed by hand), recognised as typical of liquids storage function. These findings do not allow us to conclude on the function of Fabric B, leaving open different hypotheses, such as a multifunctional use. Whereas for Fabric C, the mineralogical composition and the macroscopic features are compatible with a cooking use.

7. Summary and conclusions

The multidisciplinary approach has allowed to highlight some of the technological strategies adopted in the production of ceramic artifacts used by the Early-Middle Bronze age community of Monte Meana. The case study, being free from external influences in the ceramic production, provided a unique example of archaeometric study on local ceramic production of this period. Twenty-four ceramics were selected among the materials found in the Monte Meana cave, dated by ^{14}C to the Early-Middle Bronze age. Both macroscopic features and mineralogical composition contributed to defining five fabrics. The features observed by macroscopic analysis (morphology, surface treatments, thickness, paste composition) allowed to detect different shapes and functions of the analyzed samples. Petrographic and SEM analysis indicated several technological differences in the pottery craftwork, especially in the use of temper addiction. Spectroscopic and diffraction analyses, according to previous observations, confirmed the different functions of the vessels and the technological choices of ancient potters. Furthermore, these last techniques provided important indications about the heat treatment processes and the different thermal or mechanical stress resistances, as firing temperatures, providing additional information to hypothesise the final uses of the ceramic products.

Declarations

Author contribution statement

Giacomo Paglietti, Rita Teresa Melis, Gabriele Crucian, Marcello Franceschelli and Carla Cannas: Performed the experiments; Analyzed and interpreted the data; Wrote the paper.

Giuseppa Tanda: Conceived and designed the experiments; Contributed reagents, materials, analysis tools or data.

Anna Musinu: Conceived and designed the experiments; Analyzed and interpreted the data; Wrote the paper.

Valentina Mameli: Analyzed and interpreted the data; Wrote the paper.

Mariano Casu: Conceived and designed the experiments; Analyzed and interpreted the data; Contributed reagents, materials, analysis tools or data; Wrote the paper.

Funding statement

This work was supported by Regione Autonoma Sardegna (L.R. 7/2007 Promozione della ricerca scientifica e dell'innovazione tecnologica in Sardegna, Progetti per ricerca di base, Bando 2008: Archeometria della ceramica in Sardegna: per un protocollo di ricerca cod. CRP2_715).

The fixed-term fellowship of V. Mameli was supported by PON AIM (PON Ricerca e Innovazione 2014–2020–Azione I.2–DD n. 407 del 27 febbraio 2018 "Attraction and International Mobility", CultGeoChim project AIM1890410-3).

Data availability statement

Data included in article/supplementary material/referenced in article.

Declaration of interests statement

The authors declare no conflict of interest.

Additional information

Supplementary content related to this article has been published online at https://doi.org/10.1016/j.heliyon.2022.e09171.

Acknowledgements

We are indebted to the city of Santadi for the grant, logistical assistance and hospitality that we received. We would especially like to thank Mr. A. Pilloni and Mr. R. Cani, the president and administrator of Cantina Santadi respectively, for funding the research. A particular word of thanks also goes to Remo Forresu, the curator of the Archaeological Museum of Santadi, for his hospitality. Thanks are due to Centro Servizi di Ateneo per la Ricerca (CeSAR) for the use of the ESEM Quanta 200 manufactured by FEI equipped with a nitrogen free Thermofisher EDS–X-ray detector for SEM-EDS analysis.

References

[1] K.P. Freund, Z. Batist, Sardinian obsidian circulation and early maritime navigation in the neolithic as shown through social network analysis, J. Isl. Coast. Archaeol. 9 (2014) 364–380.

[2] C. Lugliè, L'obsidienne néolithique en Méditerranée occidentale, L'Homme Le Précieux Matières Minérales Précieuses, 2009, pp. 199–211.
[3] R.H. Tykot, Obsidian procurement and distribution in the central and western mediterranean, J. Mediterr. Archaeol. 9 (1996) 39–82.
[4] M.G. Melis, R. Cappai, L. Manca, S. Piras, The beginning of metallurgic production and the socioeconomic transformations of the Sardinian Eneolithic, in: C.C. Barbaro, C. Lemorini (Eds.), Soc. Econ. Symb. Perspect. Daw. Met. Prod. Archaeol. Reports. Int. Ser. 2372, Archaeopress Oxford, 2012, pp. 13–32.
[5] M. Pearce, The island of 'silver veins': an overwiev of the earliest metal and metalworking in Sardinia, Metalla 23.2 (2017) 91–111.
[6] J.P. Mallory, D.Q. Adams, Beaker Culture, Encycl. Indo-European Cult, 1997.
[7] G.S. Webster, M. Webster, Punctuated Insularity, The Archaeology of 4th and 3rd Millennium Sardinia 287, BAR Publishing, 2017.
[8] A. Depalmas, R.T. Melis, The nuragic people: their settlements, economic activities and use of the land, Sardinia, Italy, in: Landscapes Soc., Springer Netherlands, Dordrecht, 2010, pp. 167–186.
[9] G. Webster, The Archaeology of Nuragic Sardinia, Monographs, Equinox Publishing, 2015.
[10] W. O'Brien, Prehistoric Copper Mining in Europe, Oxford University Press, 2014.
[11] N. Cuomo di, Caprio, Ceramica in Archeologia 2, L'Erma" di Bretschneider, Roma, 2007.
[12] S.T. Levi, Dal coccio al vasaio - Manifattura, tecnologia e classificazione della ceramica, Zanichelli, Modena, 2010.
[13] M. Saracino, Prima del tornio. Introduzione alla tecnologia della produzione ceramica, Edipuglia, Bari, 2005.
[14] M.G. Gradoli, P. Waiman-Barak, T. Bürge, Z.C. Dunseth, J.H. Sterba, F. Lo Schiavo, M. Perra, S. Sabatini, P.M. Fischer, Cyprus and Sardinia in the late bronze age: nuragic table ware at hala sultan tekke, J. Archaeol. Sci. Rep. 33 (2020) 102479.
[15] R.E. Jones, P.M. Day, Late bronze age aegean and Cypriot-type pottery on sardina: identification of imports and local imitations by physico-chemical analysis, in: M.S. Balmuth (Ed.), Stud. Sardinian Archaeol. III. Nuragic Sardinia Mycenean World, Archaeopress, Oxford, 1987, pp. 257–269.
[16] L.V. Watrous, P.M. Day, R.E. Jones, The Sardinian pottery from the late bronze age site of Kommos in Crete: description, chemical and petrographical analysis and historical context, in: M.S. Balmuth, R.H. Tykot (Eds.), Sardinian Aegean Chronol. Towar. Resolut. Relat. Absol. Dating Mediterr., Oxford, 1998, pp. 337–340.
[17] R.E. Jones, S.T. Levi, M. Bettelli, Myceneans pottery in the central mediterranean: imports, imitations and derivatives, in: R. Laffineur, E. Greco (Eds.), EMPORIA Aegeans Cent. East. Mediterr. Proc. 10th Int. Aegean Conf. Aegaeum 25, 2005, pp. 539–545.
[18] R.E. Jones, S.T. Levi, M. Bettelli, L. Vagnetti, Italo-Myceneans Pottery: the archaeological and archaeometric dimensions, in: Incunabula Graeca, CNR-ISMA, Roma, 2014, pp. 1126–7348.
[19] A.B. Knapp, A. Russell, P. Van Dommelen, Cyprus, Sardinia and sicily: a maritime perspective on interaction, connectivity and imagination in mediterranean prehistory, Camb. Archaeol. J. 32 (2022) 79–97.
[20] C. Lugliè, Analisi archeometriche preliminari su elementi ceramici del Bronzo Recente dal Campidano meridionale, in: Atti Del Congr. La Civiltà Nuragica. Nuove Acquis. Quad. Atti e Monogr., 2005, pp. 155–166.
[21] B. De Rosa, G. Cultrone, M. Rendeli, Archaeometric reconstruction of Nuragic ceramics from Sant'Imbenia (Sardinia, Italy). Technological evolution of production process, Period. Mineral. 81 (2012) 313–332.
[22] M.G. Gradoli, Pottery from the underworld. A petrological analysis of a selected group of neolithic - middle bronze age ceramics from the caves of central Sardinia, in: R.B. Scott, D. Braekmans, M. Carremans, P. Degryse (Eds.), Proc. 39th Int. Symp. Archaeom., Leuven, 2012, pp. 215–222.
[23] A.M. Pollard, C.M. Batt, B. Stern, S.M.M. Young, Analytical Chemistry in Archaeology, Cambridge University Press, Cambridge, 2007.
[24] L. Carmignani, G. Oggiano, A. Funedda, P. Conti, S. Pasci, The geological map of Sardinia (Italy) at 1:250,000 scale, J. Maps 12 (2016) 826–835.
[25] G.L. Pillola, F. Leone, A. Loi, The lower cambrian Nebida group of Sardinia, in: Rend. Del Semin. Della Fac. Sci. Univ. Di Cagliari, Suppl. LXV, 1995, pp. 27–62.
[26] M. Franceschelli, S. Battaglia, G. Cruciani, S. Pasci, M. Puxeddu, Very low-temperature metamorphism in Ordovician metasedimentary rocks above and below the Sardic unconformity, SW Sardinia, Italy, Int. J. Earth Sci. 106 (2017) 531–548.
[27] C. Buosi, P. Pittau, G. Paglietti, G.G. Scanu, M. Serra, M. Ucchesu, G. Tanda, A human occupation cave during the bronze age: archaeological and palynological applications of a case study in Sardinia (western mediterranean), Archaeometry 57 (2015) 212–231.
[28] G. Paglietti, Notiziario. Monte Meana (Santadi, Prov. di Carbonia-Iglesias), Riv. Di Sci. Preist. LX, 2010, p. 393.
[29] M. Serra, S. Naitza, C. Cannas, G. Paglietti, Middle bronze age metalworking in the cave of monte Meana (south-western Sardinia, Italy), in: D. Delfino, P. Piccardo, J.C. Baptista (Eds.), Networks Trade Raw Mater. Technol. Innov. Prehistory Protohistory. An Archaeom. Approach, Proc. XVII UISPP World Congr. (1-7 Sept. 2014, Burgos, Spain) 12, Archaeopress, Oxford, 2016, pp. 1–12. /Sessione B34.
[30] G. Tanda, V. Basciu, G. Paglietti, L. Chocarro Peña, M. Ucchesu, M. Zedda, Grotta di Monte Meana (Santadi, Carbonia-Iglesias), campagne di scavo 2008-2009. Notizia preliminare, in: Atti Della XLIV Riun. Sci. Dell'Istituto Ital. Di Preist. e La Protostoria I, 2012, pp. 635–642.
[31] C.B. Ramsey, Bayesian analysis of radiocarbon dates, Radiocarbon 51 (2009) 337–360.
[32] P.J. Reimer, E. Bard, A. Bayliss, J.W. Beck, P.G. Blackwell, C.B. Ramsey, C.E. Buck, H. Cheng, R.L. Edwards, M. Friedrich, P.M. Grootes, T.P. Guilderson, H. Haflidason, I. Hajdas, C. Hatté, T.J. Heaton, D.L. Hoffmann, A.G. Hogg, K.A. Hughen, K.F. Kaiser, B. Kromer, S.W. Manning, M. Niu, R.W. Reimer, D.A. Richards, E.M. Scott, J.R. Southon, R.A. Staff, C.S.M. Turney, J. van der Plicht, IntCal13 and Marine13 radiocarbon age calibration curves 0–50,000 Years cal BP, Radiocarbon 55 (2013) 1869–1887.
[33] Munsell, Munsell Soil Color Charts, Baltimora, 2000.
[34] P.S. Quinn, Ceramic Petrography: the Interpretation of Archaeological Pottery and Related Artefacts in Thin Section, Archeopress, Oxford, 2013.
[35] G.E. De Benedetto, R. Laviano, L. Sabbatini, P.G. Zambonin, Infrared spectroscopy in the mineralogical characterization of ancient pottery, J. Cult. Herit. 3 (2002) 177–186.
[36] V.C. Farmer, Infrared Spectra of Minerals, Mineralogical Society, London, 1974.
[37] V.C. Farmer, The infra-red spectra of talc, saponite, and hectorite, Mineral. Mag. J. Mineral Soc. 31 (1958) 829–845.
[38] S. Akyuz, T. Akyuz, S. Basaran, C. Bolcal, A. Gulec, Analysis of ancient potteries using FT-IR, micro-Raman and EDXRF spectrometry, Vib. Spectrosc. 48 (2008) 276–280.
[39] R.L. Frost, The dehydroxylation of the kaolinite clay minerals using infrared emission spectroscopy, Clay Clay Miner. 44 (1996) 635–651.
[40] R. Prost, A. Dameme, E. Huard, J. Driard, J.P. Leydecker, Infrared study of structural OH in kaolinite, dickite, nacrite, and poorly crystalline kaolinite at 5 to 600 K, Clay Clay Miner. 37 (1989) 464–468.
[41] K. Omori, Analysis of the infrared absorption spectrum of diopside, Am. Mineral. 56 (1971) 1607–1616.
[42] M. Besse, J. Desideri, La diversidad Campaniforme: hábitats, sepulturas y cerámicas - bell Beaker diversity : settlements, burials and ceramics, in: M.A. Rojo Guerra, R. Garrido Pena, I. Garcia Martinez de Lagran (Eds.), El Camp. En La Península Ibérica y Su Context. Eur. - Bell Beakers Iber. Penins. Their Eur. Context., Secretariado de publicaciones e intercambio editorial Universidad de Valladolid, Valladolid, 2005, pp. 61–106. https://archive-ouverte.unige.ch/unige.
[43] O. Lemercier, La question campaniforme. The bell beaker question, in: J. Guilaine, D. Garcia (Eds.), La Protohist. La Fr. Hist. Archéologie., Hermann Editeurs, Paris, 2018, pp. 205–217.
[44] M.G. Gradoli, Bronze Age ceramics from Sardinia – a technology study, in: D. Delfino, P. Piccardo, J.C. Baptista (Eds.), Networks Trade Raw Mater. Technol. Innov. Prehistory Protohistory. An Archaeom. Approach, Proc. XVII UISPP World Congr. (1-7 Sept. 2014, Burgos, Spain) 12, 2016, pp. 69–77. /Sessione B34, Archaeopress Oxford.
[45] P.M. Rice, Pottery Analysis, A sourcebook., London, 1987.
[46] G. De Ceuninck, Forme, fonction, ethnie: approche ethnoarchéologique des céramiques du Delta intérieur du Niger (Mali), in: D. Binder, J. Courtin (Eds.), Terre Cuite Société. La Céramique, Doc. Tech. Économique, Cult., 1994, pp. 161–177.
[47] A. Mayor, Durée de vie des céramiques africaines: facteurs responsables et implications archéologiques, in: D. Binder, J. Courtin (Eds.), Terre Cuite Société. La Céramique, Doc. Tech. Économique, Cult., Editions A, 1994, pp. 179–197.
[48] J. Vieugué, Y. Garfinkel, O. Barzilai, E.C.M. van den Brink, Pottery function and culinary practices of Yarmukian societies in the late 7th millennium cal. BC: first results, Paleorient 42 (2016) 97–115.
[49] G. Rapp, Archaeomineralogy, Springer, 2009.
[50] J.G. Wilson, The addition of talc and asbestos to pot clay by past and present inhabitants of karamoja district in Uganda and adjoining districts of Kenya, Man 8 (1973) 300–302.
[51] G. Barone, P. Mazzoleni, D. Tanasi, C. Veca, La tecnologia della produzione ceramica nel Bronzo medio siciliano: il caso dei pithoi di monte san Paolillo (Catania), Riv. Di Sci. Preist. LXI (2011) 173–196.
[52] M. Zhang, Q. Hui, X.J. Lou, S.A.T. Redfern, E.K.H. Salje, S.C. Tarantino, Dehydroxylation, proton migration, and structural changes in heated talc: an infrared spectroscopic study, Am. Mineral. 91 (2006) 816–825.
[53] F. Elsass, D. Olivier, Infra red and electron spin resonance studies of clays representative of the sedimentary evolution of the Basin of Autun, Clay Miner 13 (1978) 299–308.
[54] L. Maritan, L. Nodari, C. Mazzoli, A. Milano, U. Russo, Influence of firing conditions on ceramic products: experimental study on clay rich in organic matter, Appl. Clay Sci. 31 (2006) 1–15.
[55] M. Maggetti, Composition of roman pottery from losanna (Switzerland), Br. Museum Occas. Pap. 19 (1981) 33–49.
[56] I. Daou, G.L. Lecomte-Nana, N. Tessier-Doyen, C. Peyratout, M.F. Gonon, R. Guinebretiere, Probing the dehydroxylation of kaolinite and halloysite by in situ high temperature x-ray diffraction, Minerals 10 (2020).
[57] J.G. Miller, An Infrared spectroscopic study of the isothermal deydroxylation of kaolinite at 470 °C, J. Phys. Chem. 65 (1961) 800–804.
[58] C.S. Ross, P.F. Kerr, The kaolin minerals, J. Am. Ceram. Soc. 13 (1930) 151–160.
[59] C. Manoharan, R. Venkatachalapathy, S. Dhanapandian, K. Deenadayalan, FTIR and Mössbauer spectroscopy applied to study of archaeological artefacts from Maligaimedu, Tamil Nadu, India, Indian J. Pure Appl. Phys. 45 (2007) 860–865.
[60] R. Laviano, I.M. Muntoni, Provenance and technology of apulian neolithic pottery, Geol. Soc. Spec. Publ. 257 (2006) 49–62.
[61] P. López-Arce, J. Garcia-Guinea, M. Gracia, J. Obis, Bricks in historical buildings of toledo city: characterisation and restoration, Mater. Char. 50 (2003) 59–68.
[62] S. Shoval, Using FT-IR spectroscopy for study of calcareous ancient ceramics, Opt. Mater. 24 (2003) 117–122.
[63] O.F. Tuttle, N.L. Bowen, High-temperature albite and contiguous feldspars, J. Geol. 58 (1950) 572–583.